QUADRATIC CONSTRAINT CONSISTENCY IN THE PROJECTION-FREE APPROXIMATION OF HARMONIC MAPS AND BENDING ISOMETRIES

GEORGIOS AKRIVIS, SÖREN BARTELS, AND CHRISTIAN PALUS

Abstract. We devise a projection-free iterative scheme for the approximation of harmonic maps that provides a second-order accuracy of the constraint violation and is unconditionally energy stable. A corresponding error estimate is valid under a mild but necessary discrete regularity condition. The method is based on the application of a BDF2 scheme and the considered problem serves as a model for partial differential equations with holonomic constraint. The performance of the method is illustrated via the computation of stationary harmonic maps and bending isometries.

1. Introduction

A widely used approach to discretizing partial differential equations that involve a nonlinear pointwise constraint follows [3] and is based on semi-implicit discretizations of gradient flows or evolution problems with a linearized treatment of the constraint. A corresponding projection step to guarantee an exact satisfaction of the constraint in appropriate quadrature points can only be used in special situations, e.g., if the problem is of second order and the finite element discretizations under consideration provide certain monotonicity properties; cf. [10]. However, even if the projection is stable, it may increase the residual of an approximation. It was observed in [9] that the projection step can be omitted in many situations and that the resulting constraint violation is controlled (linearly) by the step size independently of the number of iterations. We refer the reader to [8, Ch. 7] for an overview of these results. If a high accuracy in the approximation of the constraint is desired, then this limits the efficiency of the numerical method. It is the goal of this article to devise a variant of the projection-free scheme resulting from combining [3] and [9] that provides second order accuracy in the constraint violation under sharp discrete regularity conditions but is guaranteed to satisfy a first order accuracy property unconditionally. Harmonic maps serve as a model problem for partial differential equations

Date: May 1, 2024.

2010 *Mathematics Subject Classification.* 35J62 (35J50 35J57 65N30).

Key words and phrases. Harmonic maps, isometries, finite elements, iterative solution, backward differentiation formula, nonlinear bending.

with holonomic constraint, the application of our results to other problems is illustrated by the computation of bending isometries.

To explain the main ideas, we consider the numerical approximation of harmonic maps into spheres that are stationary configurations of the Dirichlet energy among unit-length vector fields for given boundary conditions, i.e.,

$$-\Delta u = \lambda u, \quad |u|^2 = 1 \text{ in } \Omega, \quad u = u_D \text{ on } \Gamma_D, \quad \partial_n u = 0 \text{ on } \partial\Omega \setminus \Gamma_D,$$

in a bounded Lipschitz domain $\Omega \subset \mathbb{R}^d$ with boundary part $\Gamma_D \subset \partial\Omega$ of positive surface measure and a given function u_D which is assumed to be equal to the trace of a function $\widetilde{u}_D \in H^1(\Omega;\mathbb{R}^\ell)$ with $|\widetilde{u}_D| = 1$ almost everywhere in Ω. The function λ is the Lagrange multiplier related to the unit-length constraint and is given by $\lambda = |\nabla u|^2$; see [8, Ch. 7] and references therein. A weak formulation determines a solution $u \in H^1(\Omega;\mathbb{R}^\ell)$ with $u = u_D$ on Γ_D and $|u|^2 = 1$ in Ω, via the equation

$$(\nabla u, \nabla v) = 0 \tag{1}$$

for all $v \in H^1_D(\Omega;\mathbb{R}^\ell)$ with $v \cdot u = 0$ in Ω, i.e., u is stationary with respect to tangential perturbations on the unit sphere along u; see, e.g., [3] or the overview in [8, Ch. 7] for details on the derivation of the weak formulation (1). The corresponding formulation as a saddle point problem has been used in various articles as a foundation for the development of approximation schemes; see, e.g., [20, 6]. In view of irregularity results for general harmonic maps, cf. [23], it is important to compute harmonic maps with low Dirichlet energy.

The iterative scheme devised in [3, 9] realizes a semi-implicit time discretization of the gradient flow problem

$$(\partial_t u, v)_\star + (\nabla u, \nabla v) = 0$$

for all $v \in H^1_D(\Omega;\mathbb{R}^\ell)$ subject to initial and boundary conditions $u(0,\cdot) = u^0$ with $|u^0|^2 = 1$ and $u|_{\Gamma_D} = u_D$, $v|_{\Gamma_D} = 0$, and the constraints

$$\partial_t u \cdot u = 0, \quad v \cdot u = 0.$$

The choice of inner product $(\cdot,\cdot)_\star$ in the gradient flow problem depends on the particular application, e.g., choosing the L^2 inner product $(\cdot,\cdot)$ yields approximation of the heat flow of harmonic maps into the sphere, while choosing the H^1_D inner product $(\nabla\cdot,\nabla\cdot)$ is well-suited for approximating stationary configurations. Particularly, with the step size $\tau > 0$ and the backward difference quotient operator $d_t u^n = (u^n - u^{n-1})/\tau$, it computes for given u^0 the sequence $(u^n)_{n=1,2,\dots}$ via the sequence of problems

$$(d_t u^n, v)_\star + (\nabla u^n, \nabla v) = 0$$

subject to homogeneous boundary conditions for $d_t u^n$ and v on Γ_D, and the linearized unit length condition

$$d_t u^n \cdot u^{n-1} = 0, \quad v \cdot u^{n-1} = 0.$$

Note that here $d_t u^n$ is seen as the unknown variable which then defines u^n via $u^n = u^{n-1} + \tau d_t u^n$. The iteration is unconditionally well posed and energy decreasing, i.e., choosing $v = d_t u^n$ yields that

$$\|d_t u^n\|_\star^2 + \frac{1}{2} d_t \|\nabla u^n\|^2 + \frac{\tau}{2} \|\nabla d_t u^n\|^2 = 0.$$

This implies the summability of the discrete time derivatives $\|d_t u^n\|_\star^2$ and hence the weak convergence of subsequences to solutions of (1). A bound for the constraint violation thus follows from the orthogonality condition and $|u^0|^2 = 1$, i.e., we have

$$|u^n|^2 - 1 = |u^{n-1}|^2 - 1 + \tau^2 |d_t u^n|^2 = \cdots = \tau^2 \sum_{j=1}^{n} |d_t u^j|^2.$$

Taking the L^1 norm of this identity, the sum on the right-hand side is bounded by $\tau(c_\star/2)\|\nabla u^0\|^2$ provided that the induced norm $\|\cdot\|_\star$ controls the L^2 norm up to a factor $c_\star^{1/2}$.

The iterative scheme can also be seen as a backward Euler method for the L^2 flow of harmonic maps if the flow metric is the L^2 inner product. For such evolution problems the discretization based on higher order time stepping methods has recently been investigated in [1]; cf. also [11] for a nodal treatment of the unit-length constraint. Provided that a sufficiently regular solution exists, quasi-optimal error estimates have been derived which imply bounds on the constraint violation. We study here the violation of the constraint in the absence of a smooth and unique solution. The use of the H^1 seminorm $\|\cdot\|_\star = \|\nabla \cdot\|$ defines an H^1 gradient flow. Being equal to the energy norm, this scalar product is natural for the minimization problem and acts as a preconditioner. This typically leads to a faster energy decay and, thus, is a preferable choice if one is interested in approximating stationary configurations.

The generalization of the semi-implicit backward Euler method for the harmonic map heat flow devised in [1] computes for given $u^0, \dots, u^{k-1}$ the sequence $(u^n)_{n=k,k+1,\dots}$ via the scheme

$$(\dot{u}^n, v)_\star + (\nabla u^n, \nabla v) = 0$$

subject to homogeneous boundary conditions on Γ_D and the linearized constraint

$$\dot{u}^n \cdot \widehat{u}^n = 0, \quad v \cdot \widehat{u}^n = 0.$$

Here $\dot{u}^n$ is a higher order approximation of the time derivative and $\widehat{u}^n$ a suitable explicit extrapolation. Adopting concepts from the construction of backward differentiation formula (BDF) methods as analyzed in, e.g., [19, 2], approximations with second order consistency properties are given by

$$\dot{u}^n = \frac{1}{2\tau}\big(3u^n - 4u^{n-1} + u^{n-2}\big),$$

or equivalently $2\dot{u}^n = 3d_t u^n - d_t u^{n-1}$, and

$$\widehat{u}^n = u^{n-1} + \tau d_t u^{n-1} = 2u^{n-1} - u^{n-2}.$$

In particular, we have that $u^n = \big(4u^{n-1} - u^{n-2} + 2\tau\dot{u}^n\big)/3$.

The iteration is initialized with one step of the linearized backward Euler method and then repeated until the discrete time-derivatives are sufficiently small or some final time $T > 0$ is reached. This initialization step does not affect the convergence behavior in the L^2 norm; cf. [24, Theorem 1.7] for related details. As an alternative in discrete settings, a first iterate that satisfies a nodal unit-length constraint exactly may be obtained by nodally projecting the backward Euler iterate to the unit sphere, or by employing a nonlinear scheme; see, e.g., [18] for a Crank-Nicolson type method. However, such approaches typically involve additional constraints, e.g., on underlying triangulations, to guarantee energy stability. Note that we always regard $\dot{u}^n$ as the unknown variable in the time steps which is then used to specify the new iterate u^n. The function $\dot{u}^n$ satisfies homogeneous boundary conditions on Γ_D if u^{n-2}, u^{n-1}, u^n equal u_D on Γ_D.

Algorithm 1.1. *Choose $u^0 \in H^1(\Omega;\mathbb{R}^\ell)$ with $u^0|_{\Gamma_D} = u_D$ and $|u^0|^2 = 1$.*
(0) Compute $d_t u^1 \in H^1_D(\Omega;\mathbb{R}^\ell)$ such that $d_t u^1 \cdot u^0 = 0$ and

$$(d_t u^1, v)_\star + (\nabla[u^0 + \tau d_t u^1], \nabla v) = 0$$

for all $v \in H^1_D(\Omega;\mathbb{R}^\ell)$ with $v \cdot u^0 = 0$; set $u^1 = u^0 + \tau d_t u^1$ and $n = 2$.
(1) Set $\widehat{u}^n = 2u^{n-1} - u^{n-2}$ and compute $\dot{u}^n \in H^1_D(\Omega;\mathbb{R}^\ell)$ with $\dot{u}^n \cdot \widehat{u}^n = 0$ and

$$(\dot{u}^n, v)_\star + \frac{1}{3}(\nabla[4u^{n-1} - u^{n-2} + 2\tau\dot{u}^n], \nabla v) = 0$$

for all $v \in H^1_D(\Omega;\mathbb{R}^\ell)$ with $v \cdot \widehat{u}^n = 0$; set $u^n = (4u^{n-1} - u^{n-2} + 2\tau\dot{u}^n)/3$.
(2) Stop if $\|\dot{u}^n\|_\star + \|d_t u^n\| \le \varepsilon_{\mathrm{stop}}$ or $n\tau \ge T$.
(3) Increase $n \to n+1$ and continue with (1).

The stopping criterion in Step (2) of the algorithm controls the residuals in the partial differential equation (1) and the involved orthogonality relation; in particular, it provides control over the difference between $\widehat{u}^n$ and u^n.

Since the subspace of functions $v \in H^1_D(\Omega;\mathbb{R}^\ell)$ satisfying $v \cdot \widehat{u}^n = 0$ in Ω is weakly closed, the Lax–Milgram lemma implies that the iteration is unconditionally well defined and terminates within a finite number of iterations. More precisely, we show in Proposition 3.2 that

$$\|\nabla \mathcal{U}^N\|_G^2 + \tau \sum_{n=2}^{N} \|\dot{u}^n\|_\star^2 \le \|\nabla \mathcal{U}^1\|_G^2,$$

where $\mathcal{U}^n = (u^n, u^{n-1})$ and $\|\cdot\|_G$ denotes a BDF-adapted variant of the L^2 norm defined in Section 2.2. An elementary calculation, cf. Proposition 3.1 below, shows that we have $\|\nabla \mathcal{U}^1\|_G \le c_G^{1/2} \|\nabla u^0\|$ so that $\dot{u}^n \to 0$ as $n \to \infty$.

For the constraint violation we show in Proposition 3.4 that for $N \geq 2$ we have

$$\||u^N|^2 - 1\|_{L^1} = \frac{3}{2}\Big(1 - \frac{1}{3^N}\Big)\tau^2\|d_t u^1\|^2 + \frac{3}{2}\tau^4 \sum_{n=2}^{N} \Big(1 - \frac{1}{3^{N+1-n}}\Big)\|d_t^2 u^n\|^2.$$

The right-hand side is always of order $O(\tau)$. Moreover, if and only if a discrete regularity property applies, i.e., if and only if $d_t u^1$ belongs to $L^2(\Omega)$ and the piecewise constant interpolant of the sequence $\tau^{1/2} d_t^2 u^n$ belongs to $L^2(0,T;L^2(\Omega))$ uniformly as $\tau \to 0$, then the right-hand side is of order $O(\tau^2)$. All of our results are stated for a semi-discrete method but hold verbatim if a spatial discretization with a nodal treatment of the (linearized) constraint is considered.

The article is organized as follows. We specify our notation and collect some auxiliary results in Section 2. In Section 3 we derive our main result. The application to the computation of harmonic maps and bending isometries is reported in Section 4. We remark that other approaches based on higher order time stepping methods for partial differential equations such as the Landau–Lifshitz–Gilbert equation typically employ a suitable projection step or make use of constraint-preserving reformulations; cf. [13, 4, 5, 15, 17, 22].

2. Auxiliary results

We use standard notation for differential operators and Lebesgue and Sobolev spaces, i.e., $H^1_D(\Omega;\mathbb{R}^\ell)$ denotes the space of vector fields $u : \Omega \to \mathbb{R}^\ell$ in $L^2(\Omega;\mathbb{R}^\ell)$ whose weak gradients are square integrable and whose traces vanish on $\Gamma_D \subset \partial\Omega$. We let $|\cdot|$ denote the Euclidean length of a vector or the Frobenius norm of a matrix and $\|\cdot\|$ the L^2 norm of a function or vector field.

2.1. **Discrete time derivatives.** We always let $\tau > 0$ denote a time-step size which gives rise to the backward difference operator

$$d_t u^n = \frac{1}{\tau}(u^n - u^{n-1})$$

for $n = 1, 2, \ldots, N$ and a sequence (u^n) in a Hilbert space. We also make use of a second discrete time derivative, defined for $n \geq 2$ by

$$d_t^2 u^n = \frac{1}{\tau^2}(u^n - 2u^{n-1} + u^{n-2}).$$

A binomial formula shows that we have

$$(d_t u^n, u^n) = \frac{d_t}{2}\|u^n\|^2 + \frac{\tau}{2}\|d_t u^n\|^2.$$

Approximations of time derivatives with higher accuracy can be obtained by a Lagrange interpolation of $k+1$ successive members of a sequence (u^n) corresponding to time levels (t_n) and a subsequent evaluation of the derivative of the interpolation polynomial at t_n. This leads to *backward differentiation*

formulas and if three successive values u^n, u^{n-1}, u^{n-2} are used, i.e., $k = 2$, provides the discrete time derivative

$$\dot{u}^n = \frac{1}{2\tau}\big(3u^n - 4u^{n-1} + u^{n-2}\big).$$

The discrete time derivatives $d_t u^n$ and $\dot{u}^n$ define equivalent ℓ^2 seminorms in the sense of the following lemma.

Lemma 2.1 (Norm equivalence)**.** *For every sequence (u^n) and $N \geq 2$ we have for the seminorms*

$$|(u^n)|_{\tau,1} = \Big(\tau \sum_{n=2}^{N} \|\dot{u}^n\|^2 + \tau\|d_t u^1\|^2\Big)^{1/2}, \quad |(u^n)|_{\tau,2} = \Big(\tau \sum_{n=1}^{N} \|d_t u^n\|^2\Big)^{1/2},$$

that $c_{12}^{-1}|(u^n)|_{\tau,1} \leq |(u^n)|_{\tau,2} \leq c_{12}|(u^n)|_{\tau,1}$ with $c_{12} \geq 1$.

Proof. The relation $2\dot{u}^n = 3d_t u^n - d_t u^{n-1}$ immediately leads to the first estimate. It also implies the second estimate since

$$\|d_t u^n\|^2 \leq \Big(\frac{2}{3}\|\dot{u}^n\| + \frac{1}{3}\|d_t u^{n-1}\|\Big)^2 \leq \frac{8}{9}\|\dot{u}^n\|^2 + \frac{2}{9}\|d_t u^{n-1}\|^2.$$

Summing over $n = 2, 3, \dots, N$ and absorbing the second sum on the right-hand side except for $\|d_t u^1\|^2$ implies the estimate. □

We also state an inverse estimate for discrete seminorms.

Lemma 2.2 (Inverse estimate)**.** *For every sequence (u^n) and $N \geq 2$ we have*

$$\Big(\tau \sum_{n=2}^{N} \|d_t^2 u^n\|^2\Big)^{1/2} \leq \tau^{-1} c_{\mathrm{inv}} \Big(\tau \sum_{n=2}^{N} \|\dot{u}^n\|^2 + \tau\|d_t u^1\|^2\Big)^{1/2}.$$

Proof. Noting that $2(\dot{u}^n - d_t u^n) = \tau d_t^2 u^n$ yields that

$$\tau\|d_t^2 u^n\| \leq 2\big(\|\dot{u}^n\| + \|d_t u^n\|\big).$$

Taking squares, summing over $n = 2, 3, \dots, N$, and incorporating Lemma 2.1 proves the estimate. □

2.2. **BDF-adapted norm.** The definition of $\dot{u}^n$ leads to the multistep scheme $\dot{y}^n = f(t_n, y^n)$ which has a second order consistency property and is referred to as a *BDF2 scheme*. It satisfies an energy stability property which is a consequence of the identity, cf. [19, p. 308],

$$\dot{u}^n \cdot u^n = d_t|\mathcal{U}^n|_G^2 + \frac{\tau^3}{4}|d_t^2 u^n|^2, \tag{2}$$

where $\mathcal{U}^n = (u^n, u^{n-1})$ for $n \geq 1$ and for an arbitrary pair $\mathcal{X} = (x, y)$ of elements x, y from an inner product space we set

$$|\mathcal{X}|_G^2 = (G\mathcal{X}) \cdot \mathcal{X} = g_{11}|x|^2 + 2g_{12}x \cdot y + g_{22}|y|^2,$$

with $g_{11} = 5/4$, $g_{12} = -1/2$ and $g_{22} = 1/4$. The positive eigenvalues $\mu_\pm = (3 \pm 2\sqrt{2})/4$ of the symmetric matrix $G = (g_{ij})$ yield the equivalence

$$\mu_-(|x|^2 + |y|^2) \le |(x,y)|_G^2 \le \mu_+(|x|^2 + |y|^2).$$

Moreover, we have $|(x,y)|_G^2 - \frac{1}{4}\big(|x|^2 + |y|^2\big) = x \cdot (x - y)$, and

$$|(x,y)|_G^2 - \frac{1}{2}|x-y|^2 = \frac{3}{4}|x|^2 - \frac{1}{4}|y|^2. \tag{3}$$

The following lemma provides a discrete version of the identity $(|v|^2)' = 2v' \cdot v$. Recall that we have $\widehat{v}^n = v^{n-1} + \tau d_t v^{n-1}$.

Lemma 2.3 (Discrete chain rule)**.** *For a sequence (v^n) and $n \ge 2$ we have*

$$2\dot{v}^n \cdot \widehat{v}^n = \frac{1}{2\tau}\Big[3|v^n|^2 - 4|v^{n-1}|^2 + |v^{n-2}|^2\Big] - \frac{3}{2}\tau^3 |d_t^2 v^n|^2.$$

Proof. We start by splitting the left-hand side of the asserted identity as

$$2\dot{v}^n \cdot \widehat{v}^n = 2\dot{v}^n \cdot v^n - 2\dot{v}^n \cdot (v^n - \widehat{v}^n).$$

We apply (2) to the first term on the right-hand side. For the second term we note that $2\dot{v}^n = 3d_t v^n - d_t v^{n-1}$ and $v^n - \widehat{v}^n = \tau(d_t v^n - d_t v^{n-1})$, and use the binomial formula $(3a-b)(a-b) = (a^2 - b^2) + 2(a-b)^2$, i.e.,

$$\begin{aligned} 2\dot{v}^n \cdot (v^n - \widehat{v}^n) &= \tau(3d_t v^n - d_t v^{n-1}) \cdot (d_t v^n - d_t v^{n-1}) \\ &= \tau\big(|d_t v^n|^2 - |d_t v^{n-1}|^2\big) + 2\tau^3 |d_t^2 v^n|^2. \end{aligned}$$

On combining the identities we deduce with $\mathcal{V}^n = (v^n, v^{n-1})$ that

$$2\dot{v}^n \cdot \widehat{v}^n = d_t\big(2|\mathcal{V}^n|_G^2 - \tau^2 |d_t v^n|^2\big) - \frac{3}{2}\tau^3 |d_t^2 v^n|^2.$$

Incorporating (3) yields the asserted identity. □

Remark 2.4. *If $\dot{u}^n \cdot \widehat{u}^n = 0$, then we deduce for $n \ge 2$ that*

$$\frac{3}{2}|u^n|^2 - 2|u^{n-1}|^2 + \frac{1}{2}|u^{n-2}|^2 = \frac{3}{2}\tau^4 |d_t^2 u^n|^2 \tag{4}$$

If $|u_\star^n|^2 = 1$ for all $n \ge 0$, then we have $2\dot{u}_\star^n \cdot \widehat{u}_\star^n = -\frac{3}{2}\tau^3 |d_t^2 u_\star^n|^2$ for $n \ge 2$.

3. Main result

We provide in this section the derivation of the identities and estimates for the energy stability and constraint violation. We always denote a pair of subsequent approximations for $n \ge 1$ via

$$\mathcal{U}^n = (u^n, u^{n-1})$$

with the iterates $(u^n)_{n=0,\dots}$ obtained with Algorithm 1.1. Throughout the following we assume that the norm induced by the inner product $(\cdot,\cdot)_\star$ controls the L^2 norm, i.e., that

$$\|v\| \le c_\star^{1/2} \|v\|_\star$$

for all $v \in H_D^1(\Omega; \mathbb{R}^\ell)$. The first result concerns the initialization step.

Proposition 3.1 (Initialization). *(a) We have*

$$\|\nabla \mathcal{U}^1\|_G^2 \le c_G \|\nabla u^0\|^2, \quad \tau \|d_t u^1\|_\star^2 \le \frac{1}{2}\|\nabla u^0\|^2.$$

(b) We have

$$\big\||u^1|^2 - 1\big\|_{L^1} = \tau^2 \|d_t u^1\|^2.$$

Proof. (a) Choosing $v = d_t u^1$ in Step (0) of Algorithm 1.1 shows that we have

$$\frac{1}{2}\|\nabla u^1\|^2 + \tau \|d_t u^1\|_\star^2 + \frac{\tau^2}{2}\|\nabla d_t u^1\|^2 = \frac{1}{2}\|\nabla u^0\|^2,$$

which implies the bounds for $\|\nabla \mathcal{U}^1\|_G^2$ and $\tau \|d_t u^1\|_\star^2$.
(b) Since $d_t u^1 \cdot u^0 = 0$ in Step (0) of Algorithm 1.1, we have that $|u^1|^2 = |u^0|^2 + \tau^2 |d_t u^1|^2$. Noting $|u^0|^2 = 1$ shows the identity. □

The second result implies that the iteration is energy decreasing and that it becomes stationary for $n \to \infty$.

Proposition 3.2 (Energy decay). *For every $N \ge 1$ we have*

$$\|\nabla \mathcal{U}^N\|_G^2 + \tau \sum_{n=2}^{N} \|\dot u^n\|_\star^2 + \frac{\tau^4}{4} \sum_{n=2}^{N} \|d_t^2 \nabla u^n\|^2 = \|\nabla \mathcal{U}^1\|_G^2.$$

Proof. Choosing $v = \dot u^n$ in Step (1) of Algorithm 1.1 yields, using (2), that

$$\tau \|\dot u^n\|_\star^2 + \|\nabla \mathcal{U}^n\|_G^2 - \|\nabla \mathcal{U}^{n-1}\|_G^2 + \frac{\tau^4}{4}\|d_t^2 \nabla u^n\|^2 = 0.$$

A summation over $n = 2, 3, \dots, N$ leads to the asserted identity. □

Remark 3.3. *For the extrapolated value $\widehat u^{n+1/2} = (3u^n - u^{n-1})/2$ we have*

$$\frac{1}{2}\|\nabla \widehat u^{n+1/2}\|^2 + \frac{1}{8}\tau^2 \|d_t u^n\|^2 = \|\nabla \mathcal{U}^n\|_G^2,$$

which yields another version of the energy law and shows that the BDF2 method has a stabilizing effect.

We next derive constraint violation estimates which provide an unconditional linear rate and a quadratic error under a mild but necessary discrete regularity condition. Qualitatively, the condition requires that sequences of approximations are uniformly bounded in $W^{1,\infty}(0,\delta;L^2(\Omega)) \cap H^{3/2}(0,T;L^2(\Omega))$ for some $\delta > 0$.

Proposition 3.4 (Constraint violation). *For every $n \ge 2$, we have*

$$|u^n|^2 = -\frac{1}{2}\Big(1 - \frac{1}{3^{n-1}}\Big)|u^0|^2 + \frac{3}{2}\Big(1 - \frac{1}{3^n}\Big)|u^1|^2 + \frac{3}{2}\tau^4 \sum_{i=2}^{n} \Big(1 - \frac{1}{3^{n+1-i}}\Big)|d_t^2 u^i|^2.$$

If $|u^0|^2 = 1$, and u^1 is computed by the linearly implicit Euler method, then $\big(|u^n|\big)$ is increasing almost everywhere in Ω and we have

$$\big\||u^n|^2 - 1\big\|_{L^1} = \frac{3}{2}\Big(1 - \frac{1}{3^n}\Big)\tau^2 \|d_t u^1\|^2 + \frac{3}{2}\tau^4 \sum_{i=2}^{n} \Big(1 - \frac{1}{3^{n+1-i}}\Big)\|d_t^2 u^i\|^2. \tag{5}$$

(a) Unconditionally and uniformly in $n \geq 1$, (5) is bounded by $c_1\tau$.
(b) If and only if for $m \geq 1$ we have

$$\|d_t u^1\|^2 + \tau^2 \sum_{i=2}^{m} \|d_t^2 u^i\|^2 \leq c_r, \tag{6}$$

then (5) is bounded by $c_2\tau^2$ for every $n = 1, 2, \ldots, m$, as $\tau \to 0$.

Proof. The main idea is to interpret (4) as an inhomogeneous linear difference equation that implies the asserted identity. The roots of the polynomial $\widetilde{\alpha}(z) = \frac{3}{2} - 2z + \frac{1}{2}z^2$ are $z_1 = 1$ and $z_2 = 3$, and thus the rational function $1/\widetilde{\alpha}$ is holomorphic in the open unit disk in the complex plane. A Taylor expansion about the origin yields for $|z| < 1$ that

$$\frac{1}{\widetilde{\alpha}(z)} = \sum_{n=0}^{\infty} \gamma_n z^n. \tag{7}$$

Multiplying this identity by $\widetilde{\alpha}(z)$ and comparing coefficients leads to the values $\gamma_0 = 2/3$ and $\gamma_1 = 8/9$, and the recursion formula

$$\frac{3}{2}\gamma_n - 2\gamma_{n-1} + \frac{1}{2}\gamma_{n-2} = 0.$$

Noting that (γ_n) is given as a linear combination of the sequences $z_1^{-n} = 1$ and $z_2^{-n} = 3^{-n}$ shows that $\gamma_n = 1 - 3^{-(n+1)}$, $n \geq 0$. We next consider the difference equation (4) with n replaced by $n - j, j = 0, \ldots, n-2$, multiply the corresponding equations by γ_j, and sum over j to derive the identity

$$\sum_{j=0}^{n-2} \gamma_j \Big(\frac{3}{2}|u^{n-j}|^2 - 2|u^{n-j-1}|^2 + \frac{1}{2}|u^{n-j-2}|^2 \Big) = \frac{3}{2}\tau^4 \sum_{j=0}^{n-2} \Big(1 - \frac{1}{3^{j+1}}\Big) |d_t^2 u^{n-j}|^2.$$

We re-arrange the left-hand side as

$$\begin{aligned}
&\sum_{j=2}^{n-2} \Big(\frac{3}{2}\gamma_j - 2\gamma_{j-1} + \frac{1}{2}\gamma_{j-2} \Big) |u^{n-j}|^2 \\
&\quad + \frac{3}{2}\gamma_0 |u^n|^2 + \Big(\frac{3}{2}\gamma_1 - 2\gamma_0 \Big) |u^{n-1}|^2 - \Big(2\gamma_{n-2} - \frac{1}{2}\gamma_{n-3} \Big) |u^1|^2 + \frac{1}{2}\gamma_{n-2} |u^0|^2,
\end{aligned}$$

and use the identities for the coefficients to deduce the asserted identity for $|u^n|^2$, which immediately leads to (5) noting that $|u^1|^2 = |u^0|^2 + \tau^2 |d_t u^1|^2$.
(a) Proposition 3.1 shows that $\tau \|d_t u^1\|^2$ is uniformly bounded. The inverse estimate of Lemma 2.2 in combination with the energy stability established in Proposition 3.2 thus proves the unconditional estimate.
(b) The assumed bound directly leads to the quadratic error estimate. It is optimal since the coefficients in (5) are uniformly bounded from below. □

Remark 3.5. *(i) Choosing the test functions $v = d_t u^1$ and $v = \dot{u}^n$ in Steps (0) and (1) of Algorithm 1.1, respectively, yields that*

$$\|d_t u^1\|_\star^2 \leq \|\nabla u^1\| \|\nabla d_t u^1\|, \quad \|\dot{u}^n\|_\star^2 \leq \|\nabla u^n\| \|\nabla \dot{u}^n\|.$$

Hence, if the norm $\|\cdot\|_\star$ controls the H^1 norm, we have that $\|d_t u^1\|_{H^1}$ and $\|\dot u^n\|_{H^1}$, $n \geq 2$, are bounded by the initial energy. Noting $2\dot u^n = 3d_t u^n - d_t u^{n-1}$ then implies a uniform bound on $\|d_t u^n\|_{H^1}$, $n \geq 1$.
(ii) If the norm $\|\cdot\|_\star$ controls the L^∞ norm, e.g., via suitable Sobolev inequalities or inverse estimates in a spatially discrete setting, then a pointwise bound for the constraint violation error can be deduced.

4. Experiments

We report in this section the performance of the devised method used as an iterative procedure to determine stationary configurations for the pointwise constrained Dirichlet energy and a nonlinear bending functional. The algorithm devised and analyzed for approximating harmonic maps into spheres can be greatly generalized and applies to the numerical solution of a constrained minimization problem

$$\text{Minimize} \quad I[u] = \frac{1}{2}a(u,u) - b(u), \quad u \in V,$$

subject to boundary conditions $\ell_{\rm bc}(u) = u_D$ and a constraint

$$G(u) = 0.$$

Given some approximation $\widehat u \in V$ satisfying $\ell_{\rm bc}(\widehat u) = u_D$ we define a corresponding linear space via

$$\mathcal{F}[\widehat u] = \big\{v \in V : \ell_{\rm bc}(v) = 0,\, g(\widehat u; v) = 0\big\},$$

where g is the derivative of G. Our algorithm then reads as follows.

Algorithm 4.1. *Choose $u^0 \in V$ with $\ell_{\rm bc}(u^0) = u_D$ and $G(u^0) = 0$.*
(0) Compute $d_t u^1 \in \mathcal{F}[u^0]$ with

$$(d_t u^1, v)_\star + a(u^0 + \tau d_t u^1, v) = b(v)$$

for all $v \in \mathcal{F}[u^0]$; set $u^1 = u^0 + \tau d_t u^1$ and $n = 2$.
(1) Set $\widehat u^n = 2u^{n-1} - u^{n-2}$ and compute $\dot u^n \in \mathcal{F}[\widehat u^n] = 0$ with

$$(\dot u^n, v)_\star + \frac{1}{3}a(4u^{n-1} - u^{n-2} + 2\tau\dot u^n, v) = b(v)$$

for all $v \in \mathcal{F}[\widehat u^n]$; set $u^n = (4u^{n-1} - u^{n-2} + 2\tau\dot u^n)/3$.
(2) Stop if $\|\dot u^n\|_\star + \|d_t u^n\|_\sharp \leq \varepsilon_{\rm stop}$ or $n\tau \geq T$.
(3) Increase $n \to n+1$ and continue with (1).

Choosing $b = 0$, $a(\cdot,\cdot) = (\nabla\cdot, \nabla\cdot)$ and $G(u) = |u|^2 - 1$ yields the setting of harmonic maps, whereas choosing $a(\cdot,\cdot) = (D^2\cdot, D^2\cdot)$ and $G(u)$ to realize an isometry constraint yields the setting of bending isometries considered below in Section 4.2. We refer the reader to [8, Section 4.3.2] for a discussion of admissible functions G that lead to a constraint violation as discussed above. The norm $\|\cdot\|_\sharp$ is assumed to be sufficiently strong to provide control over the linearization error in the constraint.

Assuming that $V = V_h$ is a finite element space, we let $\dot{\mathbf{u}}^n \in \mathbb{R}^N$ denote the coefficient vector representing $\dot{u}_h^n \in V_h$ in a suitable basis. In this case Step (1) is equivalent to the saddle point problem

$$\begin{bmatrix} \mathbf{A} & [\mathbf{G}^n]^\mathsf{T} \\ \mathbf{G}^n & 0 \end{bmatrix} \begin{bmatrix} \dot{\mathbf{u}}^n \\ \boldsymbol{\lambda} \end{bmatrix} = \begin{bmatrix} \mathbf{b} \\ 0 \end{bmatrix},$$

where $\mathbf{A} \in \mathbb{R}^{N\times N}$ encodes the bilinear form $a(\cdot,\cdot)$, $\mathbf{b}$ is a representation of the right-hand side and explicit terms, and $\mathbf{G}^n \in \mathbb{R}^{M\times N}$, $M \in \mathbb{N}$, realizes the linear constraint $g(\widehat{u}_h^n;\cdot) = 0$ with $\boldsymbol{\lambda} \in \mathbb{R}^N$ being the corresponding Lagrange multiplier. The dimension M of the discrete constraint map depends on the constraint discretization, e.g., with the restriction of a one-dimensional constraint to the vertices of a triangulation, M equals the number of vertices in the triangulation. In our implementation we employ a direct solver for the solution of the linear system in every time step to obtain $\dot{\mathbf{u}}^n$, which in turn yields a new iterate. We refer to [18, 21] for results concerning the stability of the constrained formulation and implementations based on explicit constructions of bases of the kernel of $\mathbf{G}^n$.

4.1. **Harmonic maps.** We define harmonic maps as stationary configurations for the Dirichlet energy

$$I_{\mathrm{hm}}(u) = \frac{1}{2}\int_\Omega |\nabla u|^2 \,\mathrm{d}x$$

in the set of mappings $u \in H^1(\Omega;\mathbb{R}^\ell)$ for $\Omega \subset \mathbb{R}^d$ satisfying the pointwise unit-length constraint

$$|u|^2 - 1 = 0$$

almost everywhere in Ω and the boundary condition $u|_{\Gamma_D} = u_D$ on a subset $\Gamma_D \subset \partial\Omega$ with positive surface measure. For an extension $u^0 \in H^1(\Omega;\mathbb{R}^\ell)$ of u_D, Algorithm 1.1 determines a sequence (u^n) that converges to a harmonic map of low energy. In a discrete setting we use the conforming finite element spaces

$$V_h = \mathcal{S}^1(\mathcal{T}_h)^\ell,$$

consisting of elementwise affine, globally continuous functions, and impose the initial unit-length and subsequent orthogonality relations in the nodes $z \in \mathcal{N}_h$ of the triangulation $\mathcal{T}_h$. To compute certain error quantities we employ the corresponding nodal interpolation operator $\mathcal{I}_h : C(\overline{\Omega};\mathbb{R}^\ell) \to \mathcal{S}^1(\mathcal{T}_h)^\ell$. The results established for Algorithm 1.1 carry over nearly verbatim to its discrete counterpart; cf. [10, 9]. We test its performance for a setting leading to a smooth harmonic map. Experiments for harmonic maps with singularities led to similar results.

Example 4.2 (Stereographic projection)**.** *For $d = 2$, $\ell = 3$ we set $\Omega = (-1/2, 1/2)^2$, $\Gamma_D = \partial\Omega$, and $u_D = \pi_{\mathrm{st}}^{-1}|_{\partial\Omega}$ with the inverse stereographic*

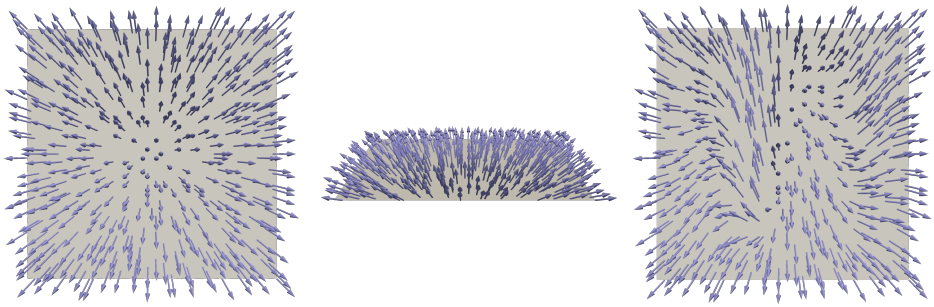

FIGURE 1. Nodal interpolant of the inverse stereographic projection π_{st}^{-1} in Example 4.2 on a coarse grid (left and middle) and perturbed initial configuration u_h^0 (right).

projection $\pi_{\mathrm{st}}^{-1} : \Omega \to S^2$ *given for* $x \in \Omega$ *by*

$$\pi_{\mathrm{st}}^{-1}(x) = (|x|^2+1)^{-1} \begin{bmatrix} 2x \\ 1-|x|^2 \end{bmatrix}.$$

Then $u = \pi_{\mathrm{st}}^{-1}$ *is a smooth harmonic map satisfying* $u|_{\partial\Omega} = u_D$.

Bounded initial data. The solution u is illustrated in the left and middle plots of Figure 1. For a spatial discretization we choose a uniform triangulation $\mathcal{T}_h$ of Ω into 8192 right-angled triangles. The initial function u_h^0 and the discrete boundary data $u_{D,h}$ are obtained via a nodal interpolation of the exact solution u and a subsequent perturbation of interior nodal values; cf. the right plot of Figure 1. For this discrete perturbation we have $I_{\mathrm{hm}}(u_h^0) \approx 22.06$ whereas the exact optimal energy is given by $I_{\mathrm{hm}}(u) \approx 3.009$.

Using step sizes $\tau = 2^{-m}$, the fixed stopping criterion $\varepsilon_{\mathrm{stop}} = 10^{-3}$ in combination with the L^2 norm that specifies $\|\cdot\|_\sharp$, and choosing the L^2 and H^1_D inner products for the gradient flow metric $(\cdot,\cdot)_\star$, respectively, we obtained the results shown in Table 1. The function u_h^{stop} denotes the iterate after N_{stop} steps for which the stopping criterion was satisfied first. The tables show the number of iterations N_{stop}, the constraint violation measure

$$\delta_{\mathrm{uni}}[u_h] = \big\| \mathcal{I}_h \left(|u_h|^2 - 1 \right) \big\|_{L^1},$$

the energy errors

$$\delta_{\mathrm{ener}}[u_h] = \big| I_{\mathrm{hm}}[u_h] - I_{\mathrm{hm}}[u] \big|,$$

and the discrete regularity quantities

$$A^2 = \tau^2 \sum_{n=2}^{N'} \|d_t^2 u_h^n\|^2, \quad B^2 = \|d_t u_h^1\|^2,$$

with $N' = N_{\mathrm{stop}}$, whose boundedness is needed to guarantee the quadratic constraint consistency results. The experimental convergence rates $\mathrm{eoc}_{\mathrm{uni}}$ and $\mathrm{eoc}_{\mathrm{ener}}$ were computed as logarithmic slopes.

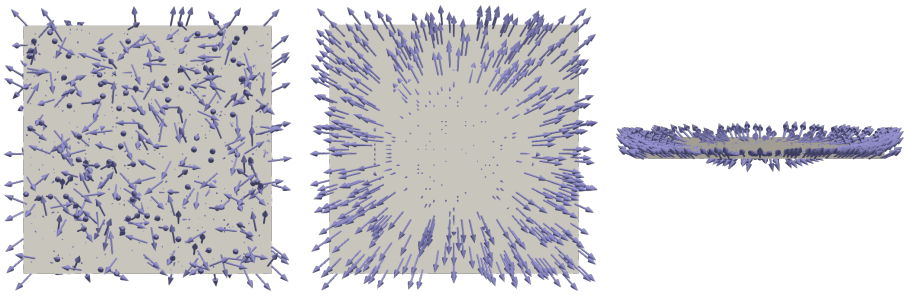

FIGURE 2. Nodal values of the rough initial data u_h^0 for the approximation of Example 4.2 on a coarse grid (left) and final iterate for the BDF2 method with $\tau = 2^{-8}$ (middle, right).

Our observations are as follows: (i) the numbers of iterations to meet the stopping criterion increase linearly with the decreasing step size and are comparable for the implicit Euler and BDF2 method as well as for the L^2 and H^1 gradient flows; (ii) the discrete regularity condition appears to be satisfied for the L^2 and H^1 gradient flows and both numerical methods, although a small growth for the quantity B^2 is observed in the case of the L^2 flows; (iii) the constraint violation and energy errors decay linearly for the implicit Euler and (nearly) quadratically for the BDF2 methods before spatial discretization errors dominate the energy error. Our explanation for (i) is that the gradient flows and stopping criteria determine times $t_\star$ at which the time derivative is sufficiently small and approximately $n \approx t_\star/\tau$ iterations are needed to reach this point via the time stepping method realized by the algorithm. While the H^1 flow provides strong control over the time derivative, cf. Remark 3.5, the rough initial data appear to lead to a certain initial growth of the first time derivative in case of the L^2 flows providing an explanation for (ii). The growth of the time derivative leads to a slight initial reduction of the quadratic convergence rate reported in (iii).

Rough initial data. As a second test problem, we reconsider Example 4.2, again choosing a uniform triangulation $\mathcal{T}_h$ of Ω into 8192 right-angled triangles. We now use randomly generated nodal values in the interior of Ω instead of a perturbation of the exact solution to initialize the discrete gradient flows, cf. Figure 2.

The initial function u_h^0 is obtained by choosing the inverse stereographic projection $u_h^0(z) = \pi_{\mathrm{st}}^{-1}(z)$ for all boundary nodes $z \in \mathcal{N}_h \cap \Gamma_D$ and choosing a random value for $u_h^0(z)$ at all interior nodes $z \in \mathcal{N}_h \cap \Omega$. This random choice is realized via generating for each interior node z two independent and uniformly distributed pseudo-random numbers $\alpha_1 \in (-\pi/2, \pi/2)$, $\alpha_2 \in (-\pi, \pi)$ that we interpret as the angles in the representation of $u_h^0(z)$ in spherical coordinates with the fixed radial distance 1. This procedure is conducted only once, such that we use the *same* randomly chosen u_h^0 for

τ	N_{stop}	$\delta_{\mathrm{uni}}[u_h^{\mathrm{stop}}]$	$\mathrm{eoc}_{\mathrm{uni}}$	A^2	B^2	$I_{\mathrm{hm}}[u_h^{\mathrm{stop}}]$	$\delta_{\mathrm{ener}}[u_h^{\mathrm{stop}}]$	$\mathrm{eoc}_{\mathrm{ener}}$
Implicit Euler method (L^2-gradient flow)								
2^{-4}	23	1.288e–01	—	1.949e+01	2.738e+01	4.667	1.658e+00	—
2^{-5}	31	1.130e–01	0.19	5.992e+01	9.432e+01	4.442	1.433e+00	0.21
2^{-6}	47	9.219e–02	0.29	1.594e+02	2.937e+02	4.133	1.124e+00	0.35
2^{-7}	78	6.867e–02	0.42	3.488e+02	7.921e+02	3.777	7.681e–01	0.55
2^{-8}	140	4.619e–02	0.57	6.077e+02	1.791e+03	3.453	4.443e–01	0.79
2^{-9}	261	2.823e–02	0.71	8.446e+02	3.375e+03	3.229	2.201e–01	1.01
2^{-10}	502	1.601e–02	0.82	9.606e+02	5.423e+03	3.108	9.877e–02	1.15
2^{-11}	982	8.627e–03	0.89	9.222e+02	7.648e+03	3.052	4.308e–02	1.19
2^{-12}	1941	4.502e–03	0.94	7.700e+02	9.734e+03	3.028	1.910e–02	1.17
2^{-13}	3858	2.305e–03	0.97	5.711e+02	1.145e+04	3.018	8.678e–03	1.13
2^{-14}	7693	1.167e–03	0.98	3.812e+02	1.272e+04	3.013	3.970e–03	1.12
BDF2 method (L^2-gradient flow)								
2^{-4}	39	2.878e–01	—	2.125e+01	2.738e+01	6.518	3.509e+00	—
2^{-5}	79	2.204e–01	0.39	5.448e+01	9.432e+01	6.493	3.484e+00	0.01
2^{-6}	39	1.615e–01	0.45	1.420e+02	2.937e+02	5.649	2.640e+00	0.40
2^{-7}	76	1.035e–01	0.64	3.229e+02	7.921e+02	4.557	1.548e+00	0.77
2^{-8}	144	5.535e–02	0.90	5.905e+02	1.791e+03	3.703	6.935e–01	1.15
2^{-9}	275	2.464e–02	1.16	8.508e+02	3.375e+03	3.245	2.356e–01	1.55
2^{-10}	534	9.370e–03	1.39	9.793e+02	5.423e+03	3.074	6.448e–02	1.86
2^{-11}	1053	3.156e–03	1.57	9.324e+02	7.648e+03	3.025	1.586e–02	2.02
2^{-12}	2096	9.710e–04	1.70	7.671e+02	9.734e+03	3.013	3.718e–03	2.09
2^{-13}	4184	2.794e–04	1.79	5.635e+02	1.145e+04	3.010	6.977e–04	2.41
2^{-14}	8363	7.647e–05	1.86	3.754e+02	1.272e+04	3.009	7.961e–05	3.13
Implicit Euler method (H^1-gradient flow)								
2^{-0}	22	5.631e–02	—	1.190e–02	3.199e–02	3.468	4.592e–01	—
2^{-1}	32	3.429e–02	0.72	1.351e–02	5.686e–02	3.236	2.265e–01	1.02
2^{-2}	53	1.921e–02	0.84	1.127e–02	8.188e–02	3.112	1.029e–01	1.14
2^{-3}	95	1.021e–02	0.91	7.554e–03	1.011e–01	3.055	4.601e–02	1.16
2^{-4}	178	5.270e–03	0.95	4.424e–03	1.133e–01	3.030	2.097e–02	1.13
2^{-5}	344	2.678e–03	0.98	2.402e–03	1.203e–01	3.019	9.751e–03	1.11
2^{-6}	677	1.350e–03	0.99	1.252e–03	1.240e–01	3.014	4.547e–03	1.10
2^{-7}	1342	6.778e–04	0.99	6.397e–04	1.260e–01	3.011	2.057e–03	1.14
2^{-8}	2672	3.396e–04	1.00	3.233e–04	1.269e–01	3.010	8.412e–04	1.29
2^{-9}	5333	1.700e–04	1.00	1.625e–04	1.274e–01	3.009	2.411e–04	1.80
2^{-10}	10655	8.503e–05	1.00	8.147e–05	1.277e–01	3.009	5.704e–05	2.08
BDF2 method (H^1-gradient flow)								
2^{-0}	16	7.048e–02	—	1.458e–02	3.199e–02	3.570	5.604e–01	—
2^{-1}	22	2.809e–02	1.33	1.735e–02	5.686e–02	3.162	1.533e–01	1.87
2^{-2}	44	9.071e–03	1.63	1.396e–02	8.188e–02	3.046	3.712e–02	2.05
2^{-3}	86	2.599e–03	1.80	8.722e–03	1.011e–01	3.018	9.086e–03	2.03
2^{-4}	171	6.991e–04	1.89	4.814e–03	1.133e–01	3.011	2.079e–03	2.13
2^{-5}	341	1.817e–04	1.94	2.515e–03	1.203e–01	3.009	2.706e–04	2.94
2^{-6}	682	4.635e–05	1.97	1.283e–03	1.240e–01	3.009	1.953e–04	0.47
2^{-7}	1363	1.171e–05	1.99	6.476e–04	1.260e–01	3.009	3.140e–04	-0.69
2^{-8}	2725	2.942e–06	1.99	3.253e–04	1.269e–01	3.009	3.440e–04	-0.13
2^{-9}	5450	7.374e–07	2.00	1.630e–04	1.274e–01	3.009	3.516e–04	-0.03
2^{-10}	10899	1.846e–07	2.00	8.160e–05	1.277e–01	3.009	3.535e–04	-0.01

TABLE 1. Step sizes, number of iterations, constraint violation, discrete regularity measures, and energy errors for the implicit Euler and BDF2 methods approximating L^2 and H^1 gradient flows for harmonic maps initialized with a perturbation of the exact solution in Example 4.2.

every step size. An interpolation of the discrete function u_h^0 on a coarse grid is illustrated in the left plot in Figure 2.

Using step sizes $\tau = 2^{-m}$, the fixed stopping criterion $\varepsilon_{\text{stop}} = 10^{-3}$ in combination with the L^2 norm that specifies $\|\cdot\|_\sharp$, and choosing the L^2 and H^1_D inner products for the gradient flow metric $(\cdot,\cdot)_\star$, respectively, we obtained the results shown in Table 2.

Partially in contrast to the first experiment with bounded initial data, we observe the following: (i) while for the H^1 flow the iteration numbers to meet the stopping criterion increase linearly with the decreasing step size, this correlation is not as pronounced for the L^2 flow; (ii) the discrete regularity condition appears to be still satisfied for the H^1 gradient flow, while it appears to be clearly violated for the L^2 flow; (iii) only the constraint violation for the H^1 flow still decays quadratically with the BDF2 method, while for the L^2 flow we only observe a rough linear convergence in the constraint, and the energies do not seem to converge at all for both flows; (iv) all iterations appear to satisfy the stopping criterion at a meta stable state of the (discrete) energy landscape as shown in the middle and right plot in Figure 2. Observation (i) underlines the preconditioning effects of the H^1 scalar product as the natural metric for the minimization problem. While the H^1 flow provides strong control over the time derivative, cf. Remark 3.5, and is less sensitive to rough initial data, (ii) shows that for the irregular initial data the regularity condition is not satisfied in the L^2 flow, which explains the constraint error behavior reported in (iii). Finally the termination at a meta stable state (iv), which is possibly caused by larger constraint errors due to the extremely high initial energies, explains the lack of energy convergence in observation (iv). We note that the occurrence of distinct meta stable states in the gradient flow appears to be related to specific random initial data and that stopping of the algorithm at such a state was also observed with the Euler method for the same initial data. With all other parameters unchanged, we did not observe this stopping phenomenon for a different set of random interior nodal values.

4.2. **Bending isometries.** Large bending deformations of thin elastic sheets can be determined via a dimensionally reduced description resulting as a Γ limit of three-dimensional hyperelasticity; cf. [16]. The variational formulation seeks a minimizing deformation for the functional

$$I_{\text{bend}}(u) = \frac{1}{2}\int_\omega |D^2 u|^2 \,\mathrm{d}x$$

in the set of functions $u \in H^2(\omega;\mathbb{R}^3)$ satisfying the pointwise isometry constraint

$$(\nabla u)^{\mathsf{T}}(\nabla u) - \mathrm{id}_{2\times 2} = 0,$$

with the identity matrix $\mathrm{id}_{2\times 2} \in \mathbb{R}^{2\times 2}$, and the boundary conditions

$$u|_{\gamma_D} = u_D, \quad \nabla u|_{\gamma_D} = \phi_D,$$

τ	N_{stop}	$\delta_{\text{uni}}[u_h^{\text{stop}}]$	eoc_{uni}	A^2	B^2	$I_{\text{hm}}[u_h^{\text{stop}}]$	$\delta_{\text{ener}}[u_h^{\text{stop}}]$	eoc_{ener}
BDF2 method (L^2-gradient flow)								
2^{-8}	718	6.133e+00	—	1.989e+05	1.824e+04	666.7	6.637e+02	—
2^{-9}	458	4.203e+00	0.55	4.908e+05	6.762e+04	714.7	7.117e+02	-0.10
2^{-10}	792	2.839e+00	0.57	1.176e+06	2.361e+05	794.2	7.912e+02	-0.15
2^{-11}	4288	1.887e+00	0.59	2.775e+06	7.526e+05	753.8	7.508e+02	0.08
2^{-12}	8206	1.195e+00	0.66	6.286e+06	2.129e+06	514.9	5.119e+02	0.55
2^{-13}	5877	6.770e-01	0.82	1.251e+07	5.261e+06	246.2	2.432e+02	1.07
2^{-14}	27184	3.296e-01	1.04	2.079e+07	1.130e+07	98.16	9.515e+01	1.35
2^{-15}	22244	1.328e-01	1.31	2.737e+07	2.111e+07	22.65	1.964e+01	2.28
BDF2 method (H^1-gradient flow)								
2^{-1}	306	2.537e-01	—	4.129e-01	1.343e-01	28.46	2.545e+01	—
2^{-2}	426	6.806e-02	1.90	3.928e-01	1.934e-01	12.00	8.994e+00	1.50
2^{-3}	837	1.439e-02	2.24	2.442e-01	2.388e-01	10.14	7.130e+00	0.34
2^{-4}	1796	3.048e-03	2.24	1.334e-01	2.677e-01	9.939	6.930e+00	0.04
2^{-5}	4048	6.702e-04	2.19	6.200e-02	2.841e-01	9.909	6.900e+00	0.01
2^{-6}	7483	1.580e-04	2.09	3.116e-02	2.929e-01	9.904	6.895e+00	0.00
2^{-7}	14849	3.832e-05	2.04	1.562e-02	2.975e-01	9.903	6.893e+00	0.00
2^{-8}	29646	9.445e-06	2.02	7.802e-03	2.998e-01	9.902	6.893e+00	0.00

TABLE 2. Step sizes, number of iterations, constraint violation, discrete regularity measures, and energy errors for the BDF2 method approximating L^2 and H^1 gradient flows for harmonic maps using random initial data in Example 4.2.

for given functions $u_D \in C(\gamma_D;\mathbb{R}^3)$ and $\phi_D \in C(\gamma_D;\mathbb{R}^{3\times 2})$. Our discretization is based on the nonconforming space of discrete Kirchhoff triangles and a discrete gradient operator, i.e.,

$$V_h = \big\{ v_h \in C(\overline{\omega};\mathbb{R}^3) : v_h|_T \in P_{3,\text{red}}(T)^3 \text{ for all } T \in \mathcal{T}_h,\\ \nabla v_h \text{ continuous in every } z \in \mathcal{N}_h \big\},$$

where $P_{3,\text{red}}(T)$ denotes a nine-dimensional subspace of cubic polynomials, and, with the space of elementwise quadratic, continuous functions $\mathcal{S}^2(\mathcal{T}_h)$,

$$\nabla_h : V_h \to \mathcal{S}^2(\mathcal{T}_h)^{3\times 2}.$$

The matrix of second derivatives D^2u in I_{iso} is replaced by the discrete second derivatives $D_h^2 u_h = \nabla\nabla_h u_h$. The isometry constraint is imposed at the nodes $z \in \mathcal{N}_h$ of the triangulation; cf. [7, 12] for related details. The discretization defines the bilinear form

$$a_h(u_h, v_h) = \int_\omega D_h^2 u_h : D_h^2 v_h \,\mathrm{d}x,$$

the linear functional

$$\ell_{\text{bc},h}(u_h) = \big(u_h|_{\gamma_D}, \nabla_h u_h|_{\gamma_D}\big),$$

and the linearized constraint functional evaluated at the nodes of the triangulation

$$g_h(\widehat{u}_h; v_h) = \big(\big[(\nabla\widehat{u}_h)^{\mathsf{T}}(\nabla v_h) + (\nabla v_h)^{\mathsf{T}}(\nabla\widehat{u}_h)\big](z)\big)_{z\in\mathcal{N}_h}.$$

Other approaches to the discretization of nonlinear bending problems such as discontinuous Galerkin methods as devised in [14] can also be formulated in this abstract way. We test Algorithm 4.1 for a setting leading to the formation of a Möbius strip.

Example 4.3 (Möbius strip)**.** *Let* $\omega = (0, L) \times (-w/2, w/2)$ *and* $\gamma_D = \{0, L\} \times [-w/2, w/2]$ *with* $L = 12$ *and* $w = 2$*. We choose boundary data* u_D *and* ϕ_D *that map the two sides contained in* γ_D *to the same interval but enforce a half-rotation of the strip* ω*.*

As initial data u^0 that is compatible with the boundary conditions and isometry constraint we use a Lipschitz continuous function that defines a flat, folded Möbius strip. The interpolated function u_h^0 on a triangulation of ω into 3072 triangles resembling halved squares is shown in Figure 3. The initial data is thus of unbounded bending energy as the mesh-size tends to zero. Using the bilinear form a_h to define discrete H^2 gradient flows determined by the implicit Euler and BDF2 methods we obtained the iterates shown also in Figure 3. The unfolding of the initially flat configuration was obtained with a forcing term in the energy that was set to zero for $t_n \geq t_f = 2$. From the coloring used for the plots in the figure we observe that the BDF2 method leads to significantly reduced constraint errors. This observation is confirmed by the numbers displayed in Table 3. For the implicit Euler and the BDF2 methods we computed the isometry constraint violation errors

$$\delta_{\mathrm{iso}}[u_h] = \big\| \mathcal{I}_h\big(|(\nabla u_h)^{\mathsf{T}}(\nabla u_h) - \mathrm{id}_{2\times 2}\,|\big)\big\|_{L^1},$$

and the discrete regularity quantities

$$A^2 = \tau^2 \sum_{n=2}^{N'} \|\nabla d_t^2 u_h^n\|^2, \quad B^2 = \|\nabla d_t u_h^1\|^2,$$

with $N' = N_{\mathrm{stop}}$. Correspondingly, we used $\|v_h\|_\sharp = \|\nabla v_h\|$ to evaluate the stopping criterion with $\varepsilon_{\mathrm{stop}} = 10^{-3}$. Our overall observations are similar to those for the approximation of harmonic maps using an H^1 gradient flow. In particular, we find that (i) the number of iterations needed to satisfy the stopping criterion grow linearly with τ^{-1} and are comparable for the implicit Euler and BDF2 methods, (ii) the constraint violation decays significantly faster for the BDF2 method than for the implicit Euler method and the discrete energies are lower, and (iii) the discrete regularity quantities remain bounded as the step sizes are reduced.

Acknowledgments. Financial support by the German Research Foundation (DFG) via research unit FOR 3013 *Vector- and tensor-valued surface PDEs* (Grant no. BA2268/6–1) is gratefully acknowledged.

References

[1] G. Akrivis, M. Feischl, B. Kovács, and C. Lubich. Higher-order linearly implicit full discretization of the Landau-Lifshitz-Gilbert equation. *Math. Comp.*, 90(329):995–1038, 2021. DOI: 10.1090/mcom/3597.

[2] G. Akrivis and C. Lubich. Fully implicit, linearly implicit and implicit-explicit backward difference formulae for quasi-linear parabolic equations. *Numer. Math.*, 131(4):713–735, 2015. DOI: 10.1007/s00211-015-0702-0.

[3] F. Alouges. A new algorithm for computing liquid crystal stable configurations: the harmonic mapping case. *SIAM J. Numer. Anal.*, 34(5):1708–1726, 1997. DOI: 10.1137/S0036142994264249.

[4] F. Alouges, E. Kritsikis, J. Steiner, and J.-C. Toussaint. A convergent and precise finite element scheme for Landau-Lifschitz-Gilbert equation. *Numer. Math.*, 128(3):407–430, 2014. DOI: 10.1007/s00211-014-0615-3.

[5] R. An, H. Gao, and W. Sun. Optimal error analysis of Euler and Crank-Nicolson projection finite difference schemes for Landau-Lifshitz equation. *SIAM J. Numer. Anal.*, 59(3):1639–1662, 2021. DOI: 10.1137/20M1335431.

[6] S. Badia, F. Guillén-González, and J. V. Gutiérrez-Santacreu. Finite element approximation of nematic liquid crystal flows using a saddle-point structure. *J. Comput. Phys.*, 230(4):1686–1706, 2011. DOI: 10.1016/j.jcp.2010.11.033.

[7] S. Bartels. Approximation of large bending isometries with discrete Kirchhoff triangles. *SIAM J. Numer. Anal.*, 51(1):516–525, 2013. DOI: 10.1137/110855405.

[8] S. Bartels. *Numerical methods for nonlinear partial differential equations*, volume 47 of *Springer Series in Computational Mathematics*. Springer, Cham, 2015, pages x+393. DOI: 10.1007/978-3-319-13797-1.

[9] S. Bartels. Projection-free approximation of geometrically constrained partial differential equations. *Math. Comp.*, 85(299):1033–1049, 2016. DOI: 10.1090/mcom/3008.

[10] S. Bartels. Stability and convergence of finite-element approximation schemes for harmonic maps. *SIAM J. Numer. Anal.*, 43(1):220–238, 2005. DOI: 10.1137/040606594.

[11] S. Bartels, B. Kovács, and Z. Wang. Error analysis for the numerical approximation of the harmonic map heat flow with nodal constraints. *IMA J. Numer. Anal.*, 44(2):633–653, June 2023. DOI: 10.1093/imanum/drad037.

[12] S. Bartels and C. Palus. Stable gradient flow discretizations for simulating bilayer plate bending with isometry and obstacle constraints. *IMA J. Numer. Anal.*, 42(3):1903–1928, 2022. DOI: 10.1093/imanum/drab050.

[13] S. Bartels and A. Prohl. Constraint preserving implicit finite element discretization of harmonic map flow into spheres. *Math. Comp.*, 76(260):1847–1859, 2007. DOI: 10.1090/S0025-5718-07-02026-1.

[14] A. Bonito, D. Guignard, R. H. Nochetto, and S. Yang. Numerical analysis of the LDG method for large deformations of prestrained plates. *IMA J. Numer. Anal.*, 43(2):627–662, 2023. DOI: 10.1093/imanum/drab103.

[15] G. Di Fratta, C.-M. Pfeiler, D. Praetorius, M. Ruggeri, and B. Stiftner. Linear second-order IMEX-type integrator for the (eddy current) Landau-Lifshitz-Gilbert equation. *IMA J. Numer. Anal.*, 40(4):2802–2838, 2020. DOI: 10.1093/imanum/drz046.

[16] G. Friesecke, R. D. James, and S. Müller. A theorem on geometric rigidity and the derivation of nonlinear plate theory from three-dimensional elasticity. *Comm. Pure Appl. Math.*, 55(11):1461–1506, 2002. DOI: 10.1002/cpa.10048.

[17] X. Gui, B. Li, and J. Wang. Convergence of renormalized finite element methods for heat flow of harmonic maps. *SIAM J. Numer. Anal.*, 60(1):312–338, 2022. DOI: 10.1137/21M1402212.

[18] J. V. Gutiérrez-Santacreu and M. Restelli. Inf-sup stable finite element methods for the Landau-Lifshitz-Gilbert and harmonic map heat flow equations. *SIAM J. Numer. Anal.*, 55(6):2565–2591, 2017. DOI: 10.1137/17M1116799.

[19] E. Hairer and G. Wanner. *Solving ordinary differential equations II: stiff and differential-algebraic problems*, volume 14 of *Springer Series in Computational Mathematics*. Springer-Verlag, Berlin, second edition, 1996, pages xvi+614. DOI: 10.1007/978-3-642-05221-7.

[20] Q. Hu, X.-C. Tai, and R. Winther. A saddle point approach to the computation of harmonic maps. *SIAM J. Numer. Anal.*, 47(2):1500–1523, 2009. DOI: 10.1137/060675575.

[21] J. Kraus, C.-M. Pfeiler, D. Praetorius, M. Ruggeri, and B. Stiftner. Iterative solution and preconditioning for the tangent plane scheme in computational micromagnetics. *J. Comput. Phys.*, 398:108866, 27, 2019. DOI: 10.1016/j.jcp.2019.108866.

[22] N. J. Mauser, C.-M. Pfeiler, D. Praetorius, and M. Ruggeri. Unconditional well-posedness and IMEX improvement of a family of predictor-corrector methods in micromagnetics. *Appl. Numer. Math.*, 180:33–54, 2022. DOI: 10.1016/j.apnum.2022.05.008.

[23] T. Rivière. Everywhere discontinuous harmonic maps into spheres. *Acta Math.*, 175(2):197–226, 1995. DOI: 10.1007/BF02393305.

[24] V. Thomée. *Galerkin finite element methods for parabolic problems*, volume 25 of *Springer Series in Computational Mathematics*. Springer-Verlag, Berlin, second edition, 2006, pages xii+370.

Department of Computer Science and Engineering, University of Ioannina, 451 10 Ioannina, Greece, and Institute of Applied and Computational Mathematics, FORTH, 700 13 Heraklion, Crete, Greece

Email address: akrivis@cse.uoi.gr

Abteilung für Angewandte Mathematik, Albert-Ludwigs-Universität Freiburg, Hermann-Herder-Str. 10, 79104 Freiburg i. Br., Germany

Email address: bartels@mathematik.uni-freiburg.de

Abteilung für Angewandte Mathematik, Albert-Ludwigs-Universität Freiburg, Hermann-Herder-Str. 10, 79104 Freiburg i. Br., Germany

Email address: christian.palus@mathematik.uni-freiburg.de

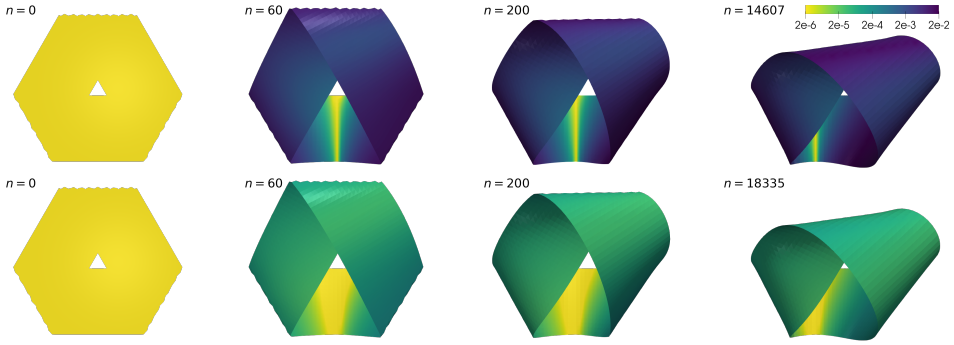

FIGURE 3. Evolution of an initially flat Möbius strip from Example 4.3 using the implicit Euler (top row) and BDF2 methods (bottom row) realizing discrete H^2-gradient flows with step sizes $\tau = 2^{-7}$. The coloring represents the constraint violation.

τ	N_{stop}	$\delta_{\text{iso}}[u_h^{\text{stop}}]$	eoc_{iso}	A^2	B^2	$I_{\text{bend}}[u_h^{\text{stop}}]$
Implicit Euler method (H_h^2-gradient flow)						
2^{-0}	349	2.255e+01	—	4.617e+02	1.054e–01	14.98
2^{-1}	198	1.342e+01	0.75	1.038e+03	1.874e–01	12.37
2^{-2}	446	5.243e+00	1.36	9.363e+02	2.699e–01	10.95
2^{-3}	874	2.493e+00	1.07	9.736e+02	3.332e–01	10.29
2^{-4}	1791	1.226e+00	1.02	8.741e+02	3.735e–01	9.983
2^{-5}	3617	6.142e–01	1.00	6.839e+02	3.965e–01	9.840
2^{-6}	7261	3.072e–01	1.00	4.351e+02	4.088e–01	9.768
2^{-7}	14538	1.538e–01	1.00	2.492e+02	4.151e–01	9.732
2^{-9}	29086	7.695e–02	1.00	1.339e+02	4.184e–01	9.715
BDF2 method (H_h^2-gradient flow)						
2^{-0}	151	5.993e+00	—	5.970e+01	1.054e–01	11.63
2^{-1}	263	6.713e+00	-0.16	2.789e+02	1.874e–01	11.04
2^{-2}	490	2.552e+00	1.40	4.090e+02	2.699e–01	10.05
2^{-3}	1049	9.924e–01	1.36	6.480e+02	3.332e–01	9.834
2^{-4}	2273	1.905e–01	2.38	4.980e+02	3.735e–01	9.727
2^{-5}	4578	4.827e–02	1.98	5.081e+02	3.965e–01	9.704
2^{-6}	9166	9.470e–03	2.35	3.986e+02	4.088e–01	9.698
2^{-7}	18313	1.506e–03	2.65	2.535e+02	4.151e–01	9.697
2^{-9}	36590	2.065e–04	2.87	1.390e+02	4.184e–01	9.697

TABLE 3. Step sizes, number of iterations, constraint violation, discrete regularity measures, and energies for the implicit Euler and BDF2 methods approximating a discrete H^2 gradient flow leading to the formation of a Möbius strip for the boundary conditions specified in Example 4.3.